

Spectrofluorimetric Hydrodynamic Voltammetry: Theory and Practice

R. G. Compton,* A. C. Fisher, R. G. Wellington, and J. Winkler

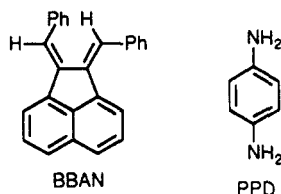
*Physical Chemistry Laboratory, Oxford University, South Parks Road, Oxford OX1 3QZ, U.K.**(Received: May 13, 1992)*

A flow cell for simultaneous spectrofluorimetric voltammetry is described. The relevant theory is presented and the sensitivity of the technique evaluated. Experiments involving (a) the photooxidation of bis(benzylidene)acenaphthene and (b) the oxidation of *p*-phenylenediamine are shown to be in good agreement with theory. It is demonstrated that the technique can reveal the existence of trace quantities of electrode reaction intermediates and products and show previously unsuspected species participating in the electrode process.

Introduction

The value of spectroscopic methods in identifying and estimating intermediates in electrochemical processes is widely recognized, and a plethora of techniques have been developed to a level of high sophistication.^{1,2} Surprisingly, in view of its high sensitivity³ and wide application in analysis, little use has been made by electrochemists of fluorescence spectroscopy except for the pioneering work of Rubim,⁴ who used an ad hoc arrangement to study Cu(I) complexes formed during the oxidation of a copper electrode. We have recently⁵ described the principles and application of an in-situ thin-layer electrode cell for fluorescence measurements on electrogenerated intermediates, and this was used to study luminescence from the radical cation of tris(4-methylphenyl)amine and the radical anion of 9,10-anthracenedione. While this approach was seen to be powerful in the qualitative investigation of the excited states of electrode intermediates, the design of the cell precluded quantitative work owing to the large size of the electrodes used in a small volume of stationary solution, experiments being essentially restricted to "stable" species. In particular, for the investigation of electrode reactions in which solution-phase species would be detected fluorimetrically, it would be desirable and essential to be able to relate the current flowing at the electrode to the intensity of the fluorescence signal induced. It will be shown in this paper that this can be readily, simply, and sensitively achieved by locating a channel flow cell inside a spectrofluorimeter and utilizing the well-defined hydrodynamic regime of the former. In this way the mass transport dependence of fluorescence signals can be readily modeled⁶ and used to identify likely mechanisms (ECE, DISP, EC', etc.) for the electrode process.

We will first describe the design of our new fluorescence flow cell, second indicate the theoretical basis on which quantitative experiments may proceed, and third apply the new methodology to two electrochemical problems. The photooxidation of bis(benzylidene)acenaphthene (BBAN) will be used to reveal the sensitivity of our protocol while the oxidation of *p*-phenylenediamine (PPD) will show that combined fluorescence/voltammetric



experiments can reveal the existence of unsuspected intermediates in familiar, well-worked electrochemical systems.⁷ In subsequent papers the use of spectrofluorimetric measurements in unraveling electrode reaction mechanisms will be examined in detail.

Cell Design

The design of the cell must be such that the following important criteria are met. First, the hydrodynamic flow must be well-defined and calculable. Second, the presence of the metallic electrode must not interfere with the fluorimetric measurements.

Third, the experimental arrangement should allow for the optimization of the sensitivity of the spectroscopic detection in any particular system.

The cell illustrated in Figure 1 meets all the above requirements. It is essentially a demountable channel electrode constructed in synthetic silica such as we have previously used for electrochemical ESR experiments. The electrode is a rectangular foil (typically 4 mm × 4 mm), for example of gold or platinum, cemented onto a silica cover plate and polished flat.⁸ Electrical connection is made to the rear of the electrode via a hole through the cover plate and the cell put together as previously described. The assembled cell is supported within a Perkin-Elmer front surface accessory (Perkin-Elmer Part 5212 3130) and used in conjunction with a Perkin-Elmer Model LS50 luminescence spectrometer. The cell position inside the spectrometer could be finely adjusted for optimum sensitivity with the front surface accessory and so that the incident exciting beam analyzed a length of solution of 9 mm × 1 mm immediately downstream of the electrode surface (see Figure 2). The width of this beam (1 mm) was significantly narrower than the electrode width (ca. 4 mm) and was positioned centrally with respect to the latter. The resulting luminescence was detected in a direction perpendicular to the incident light (Figure 2).

The flow cell was incorporated into a gravity fed all-glass flow system which permitted outgassing of the solution. Electrolyte was fed from a 250-mL reservoir via one of three capillaries for flow range setting, adjustment of flow within each range being accomplished by varying the height between the reservoir and the output tube through which spent electrolyte ran to waste. Flow rates between 10⁻¹ and 10⁻⁴ cm³ s⁻¹ were normally used. A platinum gauze counter electrode was placed downstream of the working electrode just outside the spectrometer, and a reference electrode (saturated calomel or pseudo-silver) was located upstream.

When assembled, the flow cell had cross-sectional dimensions of 6 mm × 0.4 mm and was approximately 45 mm long. The cell width was sufficiently large relative to the electrode width that "edge effects" could be neglected.⁶ At the flow rates used the flow was laminar (Reynolds number <100) and, with a lead-in length of more than a few millimeters upstream of the electrode, a parabolic (Poisseuille) velocity profile develops across the short dimension of the cell.⁹ The velocity profile across the width of the channel is, to an excellent approximation, plug flow. These hydrodynamic characteristics have been amply confirmed in numerous experiments with flow cells of the design specified.¹⁰⁻¹²

Theory

In this section the dependence of the fluorescence signal on the electrode current, the extinction coefficient of the pertinent luminescing species, the solution flow rate, and the geometrical parameters of the cell will be discussed.

The time-dependent convective-diffusive equation for a stable species of concentration *c* flowing in the channel is

$$\frac{\partial c}{\partial t} = D \frac{\partial^2 c}{\partial y^2} - v_x \frac{\partial c}{\partial x} \quad (1)$$

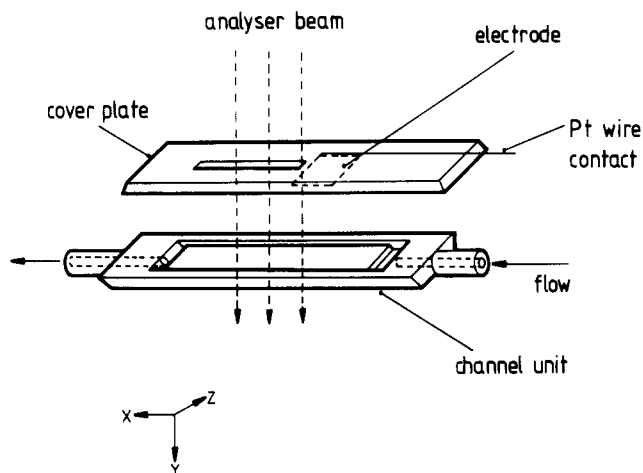


Figure 1. The channel electrode luminescence cell.

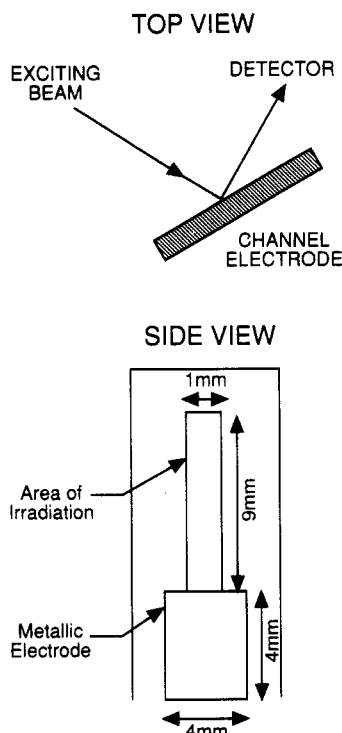


Figure 2. Schematic diagram showing the cell positioning inside the luminescence spectrometer.

where D is the diffusion coefficient, x is the distance axially along channel starting from the upstream edge of the electrode, y is the distance normal to the electrode starting from the electrode surface, and v_x is the velocity of the solution in the x direction. The neglect of diffusion in directions other than the y direction has been shown to be an excellent approximation for the experimental flow rates utilized with cells of the geometry given.¹³ Under laminar developed Poiseuille flow the velocity profile is parabolic

$$v_x = v_0 \left[1 - \frac{(h-y)^2}{h^2} \right] \quad (2)$$

where v_0 is the maximum solution velocity (cm s^{-1}) at the center of the channel and h is the half-height of the flow cell.

We have previously demonstrated that eqs 1 and 2 may be efficiently solved to provide distributions of c in time (t) and space (x, y) by means of the backward implicit finite difference method (BIFD).^{5,14} This approach has been developed to allow for the case of kinetically unstable species and for interconverting species where a series of coupled transport equations have to be solved. The computational method allows for up to 5 or 6 chemical species, each with their own diffusion coefficients, and for homogeneous

reaction rates approaching diffusional control.^{5,14-16} Adsorption-desorption and transient phenomena at electrode or other surfaces may additionally be included if necessary,¹⁷ and the extension to modeling concentration profiles downstream of the electrode presents no difficulty.¹⁸ In this way a large variety of complex electrode processes taking place at channel electrodes have been mechanistically resolved and described. In the work described below no new computation procedures are required—we refer readers to the references cited for a full description—although since the exciting beam is absorbed as it passes through the cell, we have to calculate the light intensity I at each point in the flow cell. This is accomplished by numerical integration of Beer's law

$$\partial I / \partial y = -\epsilon c I \quad (3)$$

where ϵ is the extinction coefficient in conventional units. This is readily accomplished once the concentration profiles $c(x, y, t)$ are generated using BIFD theory for a selected candidate electrode reaction mechanism assuming no photochemical decomposition is induced by the exciting beam. The intensity of the fluorescence signal may then be calculated as follows

$$S(x, y, t) = S^* \epsilon \int_{x_c}^{x_c+x_b} \int_0^{2h} \Phi I(x, y) c(x, y, t) dy dx \quad (4)$$

where Φ is the quantum yield of the fluorescence process, x_c is the electrode length, x_b is the beam length (9 mm), and S^* is a constant for the apparatus under consideration.

In this way fluorescent signal intensity $S(x, y, t)$ could be calculated as a function of electrode current and solution flow rate in the cell used for such electrode reaction mechanisms as were of interest. Computations were carried out on a Sun Sparcstation using programs written in Fortran 77, copies of which are available from the authors on request.

Experimental Section

p-Phenylenediamine (PPD; Aldrich, 99%), tetra-*n*-butylammonium perchlorate (TBAP; Fluka, purum), and acetonitrile (Fisons, dried, distilled) were used as received. Bis(benzylidene)acenaphthene (BBAN) was prepared by Dr. D. Bethell at Liverpool University according to a literature method.¹⁹ Typically experimental solutions were made up to the desired concentration in acetonitrile solution containing 0.1 M TBAP as supporting electrolyte. Solutions were degassed with oxygen-free argon prior to use.

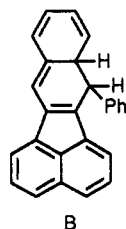
Platinum foil electrodes were supplied by Goodfellow Advanced Materials to a purity of 99.95% and thickness 0.025 mm. Channel flow cells were constructed in optical quality synthetic silica (Suprasil 2) by Heraeus Silica and Metals Ltd., Weybridge, U.K. The cover plates were cemented to the channel units using a low melting wax (Vychem Ltd., Poole, U.K.) which gave excellent adhesion to silica, melts at 50 °C, dissolves in ethanol for cell dismantling/cleaning, and gave a good seal for acetonitrile.

Electrochemical measurements employed a potentiostat and scan generator (Oxford Electrodes, Oxford, U.K.) modified to boost the counter electrode voltage.²⁰ The LS50 luminescence spectrometer was controlled by an Epson PC-AX2e personal computer, and the system was capable of measuring luminescence induced by excitation wavelengths between 200 and 800 nm. UV-vis spectra were recorded on a Perkin-Elmer lambda-5 spectrometer. Photochemical conversion of BBAN within the flow system was accomplished by focusing the output of a 20-W mercury lamp on to the glass tubing leading into the flow cell.

Results and Discussion

We consider first experiments on the photooxidation of BBAN in which a yellow solution (of BBAN in acetonitrile with 0.1 M TBAP) passing into the flow cell was photochemically partially converted into the red electrocyclic form, B, via a known photochemical route.²¹ This process was monitored amperometrically, as will be discussed below, after some preliminary experiments (without fluorescence detection) are first discussed.

In the absence of photochemical conversion of two-electron oxidation process with a half-wave potential $E_{12} = 1.23$ V (vs

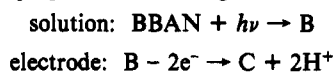


silver) was observed. Mass transport variation of the diffusion-limited current at the channel electrode enabled the calculation of the diffusion coefficient of BBAN as $D = 1.59 \times 10^{-5} \text{ cm}^2 \text{ s}^{-1}$ through application of the Levich equation

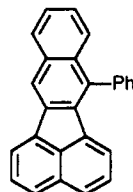
$$I_{\text{lim}} = 0.925nF[\text{BBAN}]_{\text{bulk}}w x_c^{2/3} D^{2/3} (V_f/h^2 d)^{1/3} \quad (5)$$

where F is the Faraday constant, $n = 2$, w is the electrode width, h the half-height of the channel, d the channel width, and V_f the solution flow rate ($\text{cm}^3 \text{ s}^{-1}$).

Preliminary photoelectrochemical experiments were conducted outside of the fluorescence spectrometer in which light of 377 nm from a xenon lamp was focused onto the electrode within the channel flow cell and a "prewave", cathodic of the voltammetric wave seen in the dark, was observed. This wave increased in height as the solution flow rate was reduced and the light intensity enhanced. Photocurrents corresponding to the transport-limited part of the "prewave" were measured as a function of the mass transport. The latter was analyzed in terms of the now well-established theory for a photochemical CE process²²⁻²⁴ and the mechanism unambiguously determined as such. Excellent agreement was found between theoretical and experimental photocurrents for a range of concentrations $0.29 < [\text{BBAN}] < 0.47 \text{ mM}$, the range of flow rates specified above and a factor of 5-fold in light intensity incident on the flow cell. A single rate constant of 0.59 s^{-1} for the photochemical conversion of BBAN into B (light intensity of 39.8 mW) was found to fit all the data. Accordingly we propose the following chemical transformations



where C is



This mechanism was additionally supported by the observation that cyclic voltammetry under irradiation, but with no flow, shows the formation of significant levels of protons accompanying the electrooxidation $\text{B} \rightarrow \text{C}$. The latter species was found to be highly fluorescent as shown by the spectrum in Figure 3. Under extreme conditions of very slow flow and ultrahigh light intensity, quantitative conversion under the ex situ experimental conditions could be accomplished (but not in the fluorescence work described below) from which it could be deduced, via eq 5, that B had a diffusion coefficient of $2.3 \times 10^{-5} \text{ cm}^2 \text{ s}^{-1}$.

Returning to the spectrofluorimetric voltammetry in which partial conversion of BBAN into B is accomplished by irradiation of the flow system prior to entry into the fluorescence flow cell, the current flowing at the electrode was used to determine the extent of photochemical conversion. The amount of C leaving the electrode surface was detected via fluorescence measurements. Fluorescence intensity for electrode potentials corresponding to the "prewave" was recorded as a function of mass transport and of the electrode current. Figure 4 shows how, for a fixed flow rate, the fluorescence intensity varies with generating current. It can be seen that for currents between 0 and $4.2 \times 10^{-6} \text{ A}$ a linear relationship is observed but that at higher currents a plateau is reached. The former corresponds to currents on the prewave and the latter to currents on the voltammetric wave seen in the dark.

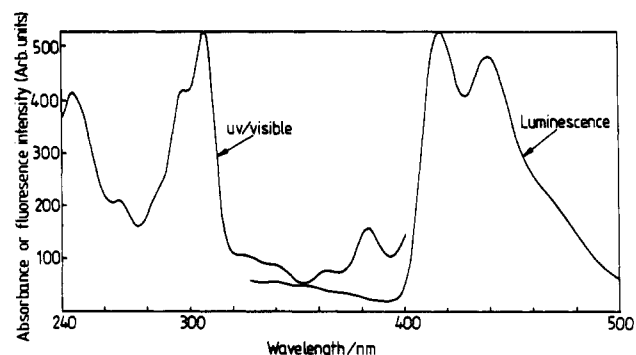


Figure 3. Absorption spectrum of C together with the luminescence spectrum resulting from excitation at 307 nm.

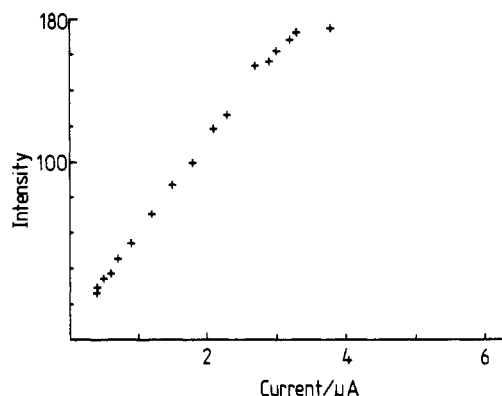


Figure 4. Variation of the fluorescence intensity (arbitrary units) as a function of the generating current as the electrode potential is swept anodically through the prewave and onto the voltammetric wave seen in the dark. Experiment performed using 0.19 mM BBAN at a flow rate of $0.29 \text{ cm}^3 \text{ s}^{-1}$ with $2h = 0.034 \text{ cm}$, $x_c = 0.451 \text{ cm}$, and $w = 0.268 \text{ cm}$.

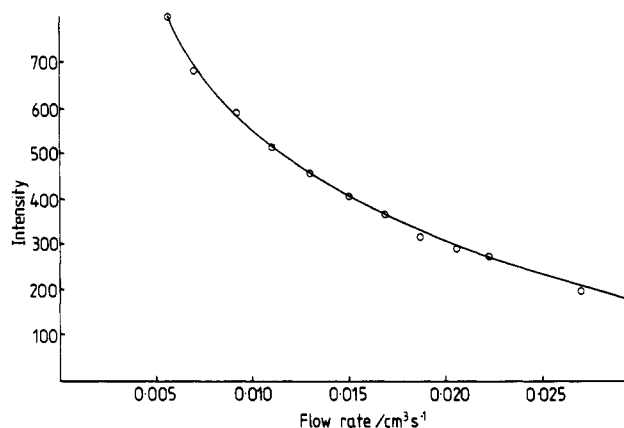


Figure 5. Variation of fluorescence intensity (arbitrary units) as a function of electrolyte flow rate for a solution containing 0.124 mM BBAN, with $x_c = 0.451 \text{ cm}$, $w = 0.268 \text{ cm}$, and $2h = 0.032$. The solid line shows the theoretical behavior calculated as specified in the text, and the circles represent the corresponding experimental data.

The figure clearly shows that while the photochemically induced prewave generates the fluorescent material C, the nature of the dark electrode process is qualitatively different and that no C is generated. Figure 5 shows the variation of the fluorescence signal intensity as a function of flow rate for the case where the electrode potential is held at a value corresponding to the transport-limited conversion of $\text{B} \rightarrow \text{C}$. Also shown is the theoretically computed behavior calculated using the BIFD method outlined above for the experimental cell geometry, the diffusion coefficients of BBAN and B as deduced above, the known extinction coefficient of C and its quantum yield for fluorescence,²⁵ and the electrode current observed for the conversion of B to C. Concentrations of BBAN up to 0.19 mM were employed, and the excellent agreement shown in Figure 5 is typical.

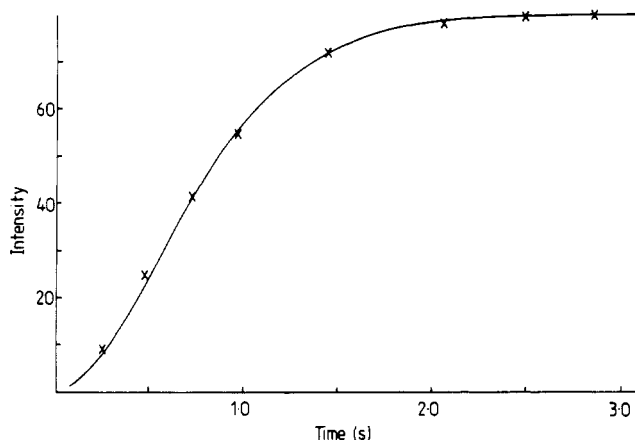


Figure 6. Experimental (×) fluorescence transient obtained at a flow rate of $0.0283 \text{ cm}^3 \text{ s}^{-1}$ and $[\text{BBAN}] = 0.476 \text{ mM}$ using a potential step of the type described in the text. The solid line indicates the theoretical transient computed using BIFD theory.

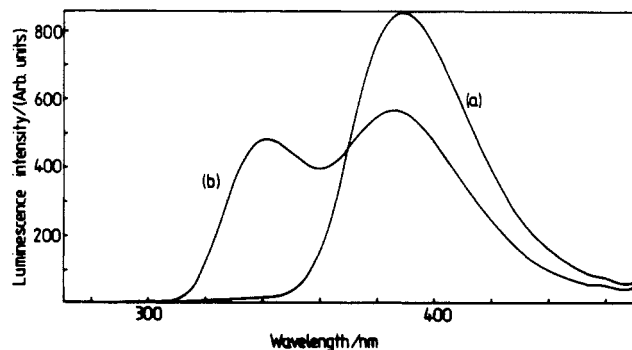


Figure 7. Luminescence spectra seen from a 0.777 mM solution of PPD (a) without electrolysis and (b) with the electrode potential held at a value corresponding to the transport-limited conversion into its radical cation.

As a further test of our model, potential step experiments were conducted in which the electrode potential was stepped from a value at which no current flowed to one corresponding to the transport-limited part of the prewave. Measurements were made at several flow rates as represented by the data shown in Figure 6. The transient was modeled using exactly the same parameters (including $S^* = 91$ relative intensity) as used in the steady-state computations. The excellent agreement seen between theory and experiment for this essentially independent set of measurements is strong confirmation of the validity of our conceptual and computational model.

It will be apparent from Figure 5, which relates to a concentration of BBAN of 0.19 mM , that the fluorescence experiment is capable of detecting very small amounts of electrogenerated material leaving the electrode surface. In particular, quantitative results were found to be possible for electrode currents as low as $0.2 \times 10^{-6} \text{ A}$ corresponding to concentrations of B as little as 0.5 nM at the electrode.

For a further independent assessment of our novel experimental arrangement, we turn now to consider the electrooxidation of PPD in acetonitrile. This has been long established as proceeding via two separate one-electron voltammetric waves, the first of which forms a radical cation, $\text{A}^{+\cdot}$.⁷ Preliminary experiments in the flow system showed results as expected, and half-wave potentials of $+0.34$ and $+0.98 \text{ V}$ (vs SCE) were estimated. Levich analysis using eq 5 gave a diffusion coefficient of $2.1 \times 10^{-5} \text{ cm}^2 \text{ s}^{-1}$, again in excellent agreement with previously reported work.²⁶

Experiments with fluorescence detection revealed the luminescent emissions shown in Figure 7. Excitations of (a) parent PPD and (b) the solution while the cation $\text{PPD}^{+\cdot}$ was being electrogenerated, using light close to 245 nm , were both found to give rise to emission. The peak luminescence of the parent was seen to be at 391 nm (optimally with 248-nm excitation) while that emitted during electrolysis was centered on 342 nm (optimally

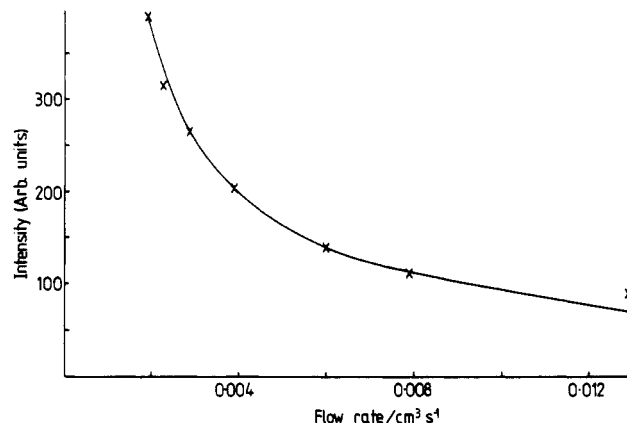
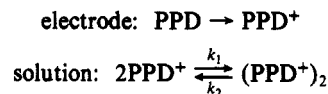


Figure 8. Variation of the fluorescence signal intensity with mass transport rate for a solution containing $[\text{PPD}] = 0.712 \text{ mM}$ and with the electrode potential set at a value corresponding to the transport-limited oxidation of PPD. The experimental geometry was $x_e = 0.618 \text{ cm}$, $w = 0.343 \text{ cm}$, and $2h = 0.0347 \text{ cm}$. Crosses represent experimental data, and the solid line shows the expected behavior computed using BIFD theory and model and parameters specified in the text.

with 243-nm excitation). The two emissions were sufficiently separated that they can be readily measured independently of each other without the need for spectral deconvolution.

Measurements were then made of the fluorescence intensity from the peak associated with electrolysis, as a function of solution flow rate and for a wide range of concentration of parent material between $0.5 \text{ mM} < [\text{PPD}] < 3 \text{ mM}$. Figure 8 shows typical results. Attempts were made to model this behavior on the initial obvious assumption that the fluorescence was due to the radical cation. However, no unique fit was found to describe all of our data sets. It was then speculated that the emission arose from the dication PPD^{2+} formed in small quantity downstream of the electrode via disproportionation of the radical cation into parent PPD and dication. This possibility was eliminated since on changing the electrode potential to a value corresponding to the second oxidation wave of PPD (where the dication is produced directly in large quantity) no substantial change in fluorescence intensity was noticed.

It is interesting that the optimum excitation wavelength of the electrolyzed solution—a wavelength at which the simple radical cation is transparent²⁷—corresponds almost exactly with the reported in the literature²⁸ for a dimeric cation species $(\text{PPD}^{+\cdot})_2$ generated at low temperature. Accordingly, the observed flow rate dependence of the fluorescence was modeled using the following kinetic scheme:



Excellent agreement, with data obtained at all flow rates and all concentrations of PPD employed, was found with the unique parameters $k_1 = 7 \times 10^3 \text{ cm}^3 \text{ mol}^{-1} \text{ s}^{-1}$ and $k_2 = 0.26 \text{ s}^{-1}$, provided that a value for $\epsilon = 3.1 \times 10^4 \text{ mol}^{-1} \text{ dm}^3 \text{ cm}^{-1}$ was assumed together with the value S^* deduced from the experiments performed on the system discussed earlier. The excellence of agreement between the theoretical mechanistic model and experiment is typified by the fit shown in Figure 8. As a further independent verification, potential step experiments were conducted, as before, and the transient fluorescent response modeled with the same parameter set. Again very good agreement was seen between theory and experiment as may be judged from Figure 9. Also shown in Figure 9 is the transient response calculated for the simpler case where the radical cation $\text{PPD}^{+\cdot}$ is the fluorescent moiety. It is very apparent that this case, with no homogeneous kinetics, offers an extremely poor fit to the experimental transient data and further justifies the selection of our chosen model in preference to the simple radical cation case. It may be concluded that the emission at 342 nm results from a dimer of the radical cation, which from the rate constants reported above

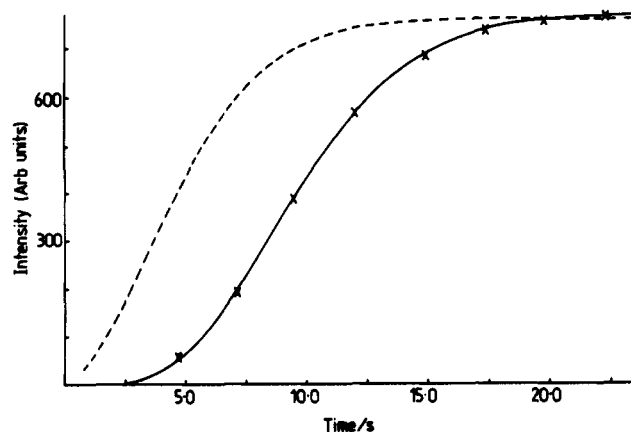


Figure 9. Experimental transient response (x) of the fluorescence intensity resulting from a potential step at a fixed flow rate $0.0038 \text{ cm}^2 \text{ s}^{-1}$. [PPD] = 2.72 mM. The solid line shows the computed time response calculated as specified in the text. The dashed line represents the theoretical time response calculated for the case of no homogeneous kinetics, all other conditions being identical.

must be present as a minority species in the solution. It is interesting to note that the combination of spectrofluorimetry and voltammetry has revealed the existence of an electrogenerated intermediate to which purely electrochemical experiments alone are blind.

Conclusions

The experiments reported above reveal spectrofluorimetric voltammetry (SFV) to be a sensitive and discriminating new technique for the quantitative investigation of complex electrode processes. Further work will be aimed at the further application of SFV to the study of electrode reactions with coupled homogeneous kinetics but also to the examination of species bound to the electrode surface.

Acknowledgment. We thank Unilever plc for financial support and Drs. D. Bethell and P. Lederer for their synthetic services.

References and Notes

- (1) Gale, R. J. *Spectroelectrochemistry*; Plenum Press: New York, 1988.
- (2) Unwin, P. R.; Compton, R. G. *Comp. Chem. Kinet.* **1989**, *29*, 173-290.
- (3) Kroog, P. A. *Principles of Instrumental Analysis*; Saunders College Publishing: 1985.
- (4) Rubim, J. C.; Gutz, I. G. R.; Sala, O. *Chem. Phys. Lett.* **1984**, *111*, 117.
- (5) Compton, R. G.; Fisher, A. C.; Wellington, R. G. *Electroanalysis* **1991**, *3*, 27-29.
- (6) Compton, R. G.; Pilkington, M. B. G.; Stearn, G. M. *J. Chem. Soc., Faraday Trans. 1* **1988**, *84* (6), 2155.
- (7) Adams, M.; Blois, M. S.; Sands, R. H. *J. Chem. Phys.* **1988**, *28*, 744.
- (8) Compton, R. G.; Coles, B. A. *J. Electroanal. Chem.* **1983**, *144*, 87.
- (9) Levich, V. G. *Physicochemical Hydrodynamics*; Prentice-Hall: Englewood Cliffs, NJ, 1962.
- (10) Compton, R. G.; Unwin, P. R. *J. Electroanal. Chem.* **1986**, *206*, 57.
- (11) Compton, R. G.; Sealy, G. R. *J. Electroanal. Chem.* **1983**, *145*, 35.
- (12) Compton, R. G.; Page, P. J.; Sealy, G. R. *J. Electroanal. Chem.* **1984**, *161*, 129.
- (13) Flannagan, J. B.; Marcoux, L. *J. Phys. Chem.* **1974**, *78*, 718.
- (14) Fisher, A. C.; Compton, R. G. *J. Phys. Chem.* **1991**, *95*, 7538.
- (15) Compton, R. G.; Coles, B. A.; Pilkington, M. B. G.; Bethell, D. *J. Chem. Soc., Faraday Trans. 1* **1990**, *86*, 663.
- (16) Fisher, A. C.; Compton, R. G. *J. Appl. Electrochem.* **1991**, *21*, 208.
- (17) Compton, R. G.; Wilson, M. *J. Appl. Electrochem.* **1990**, *20*, 793.
- (18) Compton, R. G.; Fisher, A. C.; Wellington, R. G.; Bethell, D.; Lederer, P. *J. Phys. Chem.* **1991**, *95*, 4749.
- (19) Maxim, M. *Bull. Soc. Chim.* **1928**, *43*, 709.
- (20) Compton, R. G.; Waller, A. M. *J. Electroanal. Chem.* **1985**, *195*, 289.
- (21) Müller, M. *Liebigs Ann. Chem.* **1972**, *16*, 758.
- (22) Compton, R. G.; Fisher, A. C.; Wellington, R. G.; Bethell, D. *Electroanalysis* **1991**, *3*, 183.
- (23) Compton, R. G.; Coles, B. A.; Stearn, G. M.; Waller, A. M. *J. Electroanal. Chem.* **1985**, *191*, 15.
- (24) Fisher, A. C.; Coles, B. A.; Compton, R. G.; Bethell, D.; Tripathi, S. *J. Chem. Soc., Faraday Trans.* **1990**, *86*, 3603.
- (25) Ginter, H.; Heinrich, G. *J. Photochem.* **1982**, *18*, 9.
- (26) Kapturkiewicz, A.; Jaenicke, W. *J. Chem. Soc., Faraday Trans. 1* **1987**, *83*, 2727.
- (27) Nakayama, S.; Suzuki, K. *Bull. Chem. Soc. Jpn.* **1973**, *46*, 3694.
- (28) Kimura, K.; Yamada, H.; Tsubomura, H. *J. Chem. Phys.* **1968**, *48*, 440.

Direct Observation of Three-Dimensional Transformation of Insoluble Monolayers

S. Siegel,[†] D. Hönig,[‡] D. Vollhardt,^{*†} and D. Möbius[†]

Max-Planck-Institut für Kolloid- und Grenzflächenforschung, Rudower Chaussee 5, D-1199 Berlin, Germany, and Max-Planck-Institut für Biophysikalische Chemie, Am Fassberg, D-3400 Göttingen, Germany (Received: February 1, 1992; In Final Form: April 23, 1992)

Nucleation and growth of three-dimensional crystallites in fatty acid monolayers at constant pressure have been studied by direct visualization using a Brewster angle microscope. The number of growing nuclei depends on the film pressure, and the shape depends on the composition of the subsolution. At $\text{pH} \leq 3$ single crystallites are formed with an area of more than 0.1 mm^2 and a thickness of ≤ 6 layers.

Introduction

The stability or instability of insoluble monolayers has been a subject of major interest. In the metastable region, i.e., at surface pressures between the equilibrium spreading pressure and the so-called "collapse pressure", the monolayers show relaxation phenomena either as a decrease in surface pressure (π) with time at constant mean molecular area (A) or as a decrease of A with time at constant π . Constant-pressure relaxation of metastable monolayers represents the basis for defined modeling the trans-

formation of monolayer material to 3D structures.

Recently a nucleation/growth model has been introduced¹⁻³ to describe theoretically the constant-pressure monolayer relaxation on the basis of nucleation and subsequent growth of the nuclei considering the overlap of the growing nuclei. Good agreement of the adequate nucleation/growth mechanism with the time-dependent area relaxation has been obtained for the whole range of constant-pressure relaxations of insoluble monolayers. But no information could be provided concerning the surface morphology at the micrometre level.

Fluorescence microscopy^{4,5} may give insight into the lateral structure of monolayers; however, a fluorescent probe is necessary. In such cases, the possibility of an effect of the probes on nucleation and growth cannot be excluded.

[†]Max-Planck-Institut für Kolloid- und Grenzflächenforschung.

[‡]Max-Planck-Institut für Biophysikalische Chemie.